



Rapid post-earthquake damage assessment of building portfolios through deep learning-based component-level image recognition

De-Cheng Feng ^a, Xin Yi ^b, Zeynep Tuna Deger ^c, Han-kun Liu ^d, Shi-Zhi Chen ^{e,*},
Gang Wu ^a

^a Key Laboratory of Concrete and Prestressed Concrete Structures of the Ministry of Education, Southeast University, Nanjing, 211189, China

^b School of Civil Engineering, Southeast University, Nanjing, 211189, China

^c Earthquake Engineering and Disaster Management Institute, Istanbul Technical University, Istanbul, 34467, Turkey

^d Sichuan Institute of Building Research, Chengdu, 610081, China

^e School of Highway, Chang'an University, Xi'an, 710064, China



ARTICLE INFO

Keywords:

Deep learning
Image classification
Structural assessment
Component image
Global damage level

ABSTRACT

Frequent seismic events significantly heighten the likelihood of the building structure being impacted throughout its operational lifecycle. Seismic effects on these structures result in a notable reduction in structural safety and serviceability. Enabling the post-earthquake recovery of building structures necessitates a precise and swift assessment of earthquake-induced damage. The conventional method for assessing building damage involves collecting data through close manual observation or contact inspection. Although it can obtain relatively accurate results by combining evaluation specifications, it is time-consuming and labour-intensive. Deep learning (DL) is data-driven and employs computational methods for data processing. The image classification function of convolutional neural network (CNN) in DL brings great convenience to image data processing. It has been applied to various aspects of structural health monitoring/post-disaster assessment. However, most of the current studies focus on the component level and lack of a comprehensive perspective on the whole structure, which is not conducive to the judgment of the overall condition. Consequently, this paper proposes a rapid assessment method of the overall damage level of post-earthquake buildings based on component images and DL. Two component-level image classification models, component type and damage level, are firstly trained. Then, the images of the buildings to be evaluated after the earthquake are collected and classified. Combined with the weights of different component types and damage levels proposed, the overall condition scores and grades of the structures can be obtained by weighted calculation. The proposed method realizes an overall evaluation of the structural damage condition after seismic events, and further extends to the building portfolios, providing actionable guidance for subsequent personnel and fund allocation, rescue, and maintenance measures. Due to limitations in the dataset, such as the potential biases in the training dataset, the trained model is not perfect and faces challenges in distinguishing between minor and moderate damage. In the future, the dataset should update and ideally cover a wide range of building types, component types, and damage levels to ensure the model's robustness and applicability to various real-world scenarios.

* Corresponding author.

E-mail addresses: dfeng@seu.edu.cn (D.-C. Feng), 220211313@seu.edu.cn (X. Yi), zeynep.tuna@itu.edu.tr (Z.T. Deger), lhksibr@foxmail.com (H.-k. Liu), szchen@chd.edu.cn (S.-Z. Chen), g.wu@seu.edu.cn (G. Wu).

1. Introduction

Earthquake is a natural disaster phenomenon that generates ground vibrations within a specific range due to seismic waves resulting from abrupt ruptures in the Earth's crust. The seismic events in China, observed in 1976 and 2008, significantly impacted both human safety and property. Lately, earthquakes in Albania, Croatia and Turkey have caused significant loss of life and socio-economic damage [1–3]. During the lifespan of buildings, there will be different degrees of damage due to the impact of earthquake. If the structure is damaged lightly, it will affect the regular use function and cannot meet the daily use needs. Severe damage can result in structural deterioration, leading to excessive deformation, cracking, concrete spalling, and even structural collapse, which directly causes economic losses and personal safety problems. The conventional methods of post-earthquake damage assessment are mainly manual sampling, or sampling combined with a detector, and then combine with relevant norms and expert experience to form a quality inspection report. However, such an approach demands proficiency from inspectors and can be influenced by their subjective judgments. In addition, the considerable quantity and wide distribution of buildings requiring post-earthquake assessment makes the conventional inspection method time-consuming and labor-intensive.

Machine learning (ML), as an important subfield of AI, relies on data-driven techniques and computer processing, which greatly improves the efficiency and accuracy of data processing [4–11]. Image classification is one of the basic tasks of computer vision (CV), which means that given an image, the computer uses algorithms to find the category label to which it belongs. The conventional image classification algorithm extracts color, texture, space, and other features of the image, which is suitable for simple tasks, but unsatisfactory in complex image classification tasks. DL, a subset of ML, seeks to simulate human neural network system to build deep artificial neural network, analyze and interpret the input data, and combine the low-level features of the data into abstract high-level features [12]. DL has proved indispensable in AI domains such as CV and Natural Language Processing (NLP) [11]. As a typical representative of DL, CNN excels in CV tasks. In contrast to conventional image classification algorithms that require manual feature extraction, CNN uses convolutional operations to extract features directly from input images. They effectively learn feature representations from abundant samples and possess enhanced model generalization capability. CNN can be employed to discern the structural damage condition from images of post-earthquake-affected buildings, which facilitates rapid image-based predictions of building health conditions. This not only saves the huge workload resulting from repeated calculations but also enables reasonable allocation of subsequent detection tasks while maintaining a certain level of accuracy. This effectively maximizes the detection efficiency and reduces the loss caused by the untimely detection of dangerous buildings.

LeNet, proposed by LeCun et al. [13] in 1998, stands as the earliest CNN model. It primarily targets handwritten digit recognition in the MNIST (modified NIST) dataset, thereby establishing the groundwork for the evolution of CNN. In 2012, Krizhevsky et al. [14] proposed AlexNet, which employs the rectified linear unit (ReLU) as its activation function. The inclusion of local response normalization (LRN) addresses the issue of gradient vanishing. The overfitting problem is greatly alleviated by using data augmentation and dropout. The training speed is improved by using two GPUs in parallel computation. At the 2012 ImageNet competition, AlexNet outperformed its closest competitor by a substantial margin, securing the top spot in the classification task. AlexNet has greatly improved the performance of tasks such as image classification, making CNN gradually become a research hotspot in the field of CV. Subsequently, VGGNet (Visual Geometry Group) [15] and GoogLeNet [16] have been proposed successively. CNN continues to make breakthroughs in image classification tasks, and the increase of network depth improves its feature extraction capability. However, with the increase of network depth, the issue of gradient vanishing becomes more and more serious, and the optimization of the network becomes more and more challenging. Subsequently, in 2016, He et al. [17] introduced residual convolutional neural networks (ResNet), which further increased network depth and enhanced the performance of image classification tasks. In 2017, Huang et al. [18] proposed a dense connected convolutional neural network, which uses a simple connection pattern where all layers are directly connected to further enhance information propagation in the network. In recent years, several lightweight networks with limited parameter volumes and low computational complexity have been introduced. Lightweight networks require less cross-server communication during training, demand lower transmission bandwidth when transferred to devices such as autonomous driving cars, and can be accommodated on hardware with limited memory capacity. Typical lightweight networks are SqueezeNet [19], Xception [20], MobileNet series [21,22], ShuffleNet series [23] and EfficientNet series [24].

AI-based technologies have long been combined with civil engineering [25,26]. ML-based CV techniques have been employed in structural health monitoring [27,28]. In 2016, Cha et al. [29] detected loose bolts based on steel bolt images. In 2018, Cha et al. [30] utilized steel and concrete components to identify concrete cracks, steel bar rust, bolt rust, and steel bar stripping. In 2018, Gao and Mosalam [31] used a variety of building systems and components to classify structural components and systems, damage types and levels. In 2018, Kucuksubas and Sorgucu [32] identified cracks in reinforced concrete buildings based on image data. In 2019, Hoang et al. [33] detected spalling of reinforced concrete based on images of reinforced concrete building components. In 2020, Gonzalez et al. [34] used multiple building-type images to identify building materials and types of lateral support systems. In 2020, Naito et al. [35] used images of multiple building types to identify earthquake damage levels. In 2023, Dogan et al. [36] developed a deep transfer learning algorithm, which allowed distinguishing of damages caused by corrosion from earthquake-induced damages in structural elements of RC buildings. It can be seen that intelligent inspection methods based on image data have been used to detect cracks and spalling in reinforced concrete, to detect loosening and corrosion of steel bolts, and to identify and classify structural and component types as well as the presence and severity of damage.

However, the majority of the current research focus on the local parts of the structure, such as crack identification, component damage level determination and so on. Although these studies can identify the local damage characteristics of the structure accurately, they lack the overall grasp of the structure. However, it is vital for the inspection department to comprehensively understand the

overall condition of the damaged building structure, which has important guiding significance for the subsequent deployment of personnel and funds, and the response of maintenance responses. Bai et al. [37] introduced a method for assessing damage in reinforced concrete structures from individual components to the entire structure, but a substantial number of images needed to be collected and involved a complex calculation process. Du et al. [38] introduced a rapid loss assessment method for post-earthquake building portfolios based on InSAR following the 2023 Turkey earthquake. This method directly assesses buildings at the regional scale, but it has high requirements for devices. Bektas et al. [39] introduced a neural network-based rapid visual screening method for reinforced concrete, adobe mud, bamboo, brick, stone, and timber buildings.

Under the guidance of comprehensive and rapid access to the overall structure condition, this paper proposes an overall building condition assessment method based on component images and DL methods. By integrating the information of component types and damage levels into the overall structure condition score, the overall comprehension of the post-earthquake building structure condition level can be realized. It can be further extended from single to building portfolios, which can be scientific guidance for subsequent rescue and maintenance operations, personnel and fund deployment.

The sections in this article are organized as follows: Section 2 introduces the methodology and innovation points of this paper. Section 3 introduces the source of the image classification dataset used in this paper, the image classification task, and the models and algorithms for image classification. Section 4 introduces the methods and steps of rapid assessment of the overall condition of the structure based on component image and DL. Section 5 verifies the rationality and applicability of the proposed method through an actual engineering case. Section 6 summarizes the conclusions, limitations, and future research directions of the proposed method.

2. Methodology for rapid damage assessment of building portfolios

The main objective of this study is to propose a method that carries out a rapid evaluation of post-earthquake global damage level of concrete building based on component image and DL. This method involved two aspects, i.e., (1) collect the images of all components for a building structure and then use DL model to identify the component type and damage extent. (2) calculating the overall damage score of the building by a weighted sum of the classification results for all components. Hence, the inputs are the images of all the components while the output is an overall score of the building.

In this regard, two factors are important, say, the DL model that can classify both the component type and damage level, and the determination of the weights for the component type and damage extent. Fig. 1 illustrates the framework of the proposed methodology that is implemented through the following five stages:

- Stage 1 – Image acquisition and preprocessing. Images of components from post-earthquake buildings requiring evaluation are collected. Further details are presented in Section 4.2.1.
- Stage 2 – Image classification. Two image classification tasks are implemented based on corresponding datasets. The image classification models of component type and damage level are obtained based on DL and transfer learning. Further details are presented in Section 3.
- Stage 3 – Component classification results. The images of components from post-earthquake buildings that need evaluation are input to models, yielding component type classification and damage level classification results. The results of component type classification and damage level classification are visualized. Further details are presented in Section 4.2.2.
- Stage 4 – Structural condition calculation. Different weights are assigned to different component types and damage levels according to specifications and actual engineering experience. According to the quantity and weight of classification results, a weighted

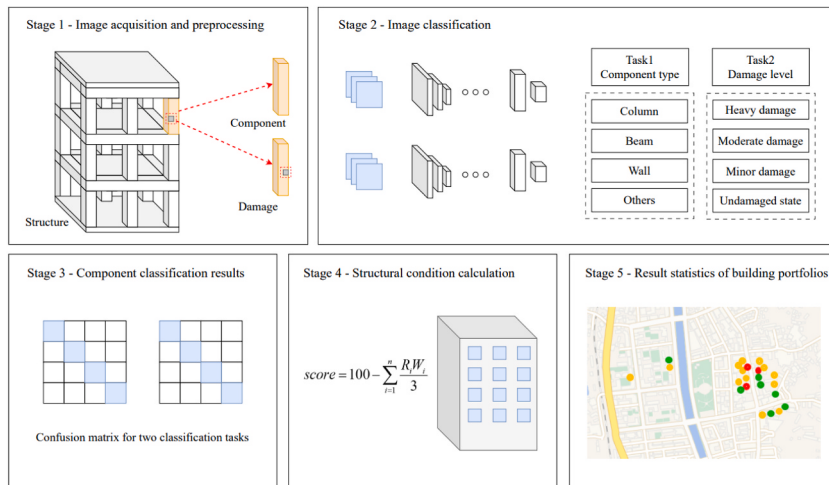


Fig. 1. Rapid damage assessment procedures for building portfolios.

analysis is performed to derive an overall condition score for the structure. The overall score, along with classification threshold scores, is then utilized to ascertain the structural condition level. Further details are presented in Section 4.2.2.

- Stage 5 – Result statistics of building portfolios. Based on the structural condition level and map information, the calculation results are visualized.

The method proposed in this paper overcomes the limitations of previous studies that only focus on local damage, determination of structure type, and collapse judgment [29–35]. By comprehensively considering the types and damage levels of components, this study utilizes images of local building components to predict the overall condition level of post-earthquake buildings. The damage identification is expanded from component level to structure level based on weighted calculation, and the condition level of post-earthquake structures is captured from a global scale. The post-earthquake condition of the building portfolios in a certain area can also be obtained. The buildings in urgent need of maintenance were screened out to further provide guidance for follow-up response.

3. Component-level damage assessment using deep learning

3.1. Component-level damage assessment by image recognition

Following the guidelines outlined in GB/T 24,335–2009 “Classification of earthquake damage to buildings and special structures” [40], the classification of building damage levels is accomplished through a sequence of steps: Initial classification of buildings is based on their structural types; distinction is then made between load-bearing and non-load-bearing building components, and their respective damage levels are evaluated; subsequently, the damage level of the building is determined based on the level of damage to each component, the complexity of repair, and the extent of loss in structural functionality.



Fig. 2. Classification of component types in ImageNet [31,42] This image classification task contains a total of 5334 images, with 1823 for columns, 571 for beams, 2533 for walls, and 407 for others. Each category is randomly divided into training set, validation set, and test set in the ratio of 8:1:1.

The JGJ/T415-2017 “Technical specification for post-earthquake urgent assessment and repair of buildings” [41] outlines the fundamental principles for the classification of earthquake damage levels in buildings, adhering to the following guidelines: For various types of buildings, earthquake damage levels should be divided according to different structural characteristics; the primary consideration when evaluating a building’s earthquake damage level should be directed toward its load-bearing components; incorporating a quantitative framework is essential for gauging the extent of earthquake-induced damage in buildings; the classification of earthquake damage levels should encompass factors such as repair complexity, usability, and direct economic losses; furthermore, the classification process must reflect the immediate earthquake-related harm sustained by buildings, excluding any damage incurred by other factors prior to the earthquake.

Considering the aforementioned specifications comprehensively, it can be inferred that classifying component types and component damage levels is necessary. Therefore, appropriate criteria need to be established for these two classification tasks. Gao et al. [42] developed the PEER Hub ImageNet (ϕ -net), which contains images related to structural engineering, such as buildings, bridges, etc. There are both damaged and undamaged states in the collected images. The ϕ -net, initially comprising 2000 images, has been expanded to encompass 36,413 images, establishing a robust framework featuring 8 primary tasks. Two classification tasks, component type and damage level, are included in an eight-task framework. Consequently, the datasets associated with component type and damage level within the ϕ -net framework can be effectively employed for training image classification models.

It should be noted that the vast majority of civil building structures consist of low-rise reinforced concrete frame structures and brick-concrete structures. The method proposed in this paper is suitable for low-rise civil buildings.

3.1.1. Task 1: component type classification

Within a structural system, distinct structural components fulfill varying roles. Vertical components, such as columns, provide lateral stiffness to resist lateral forces caused by earthquakes, while horizontal members, such as beams, partitions and joints, transfer

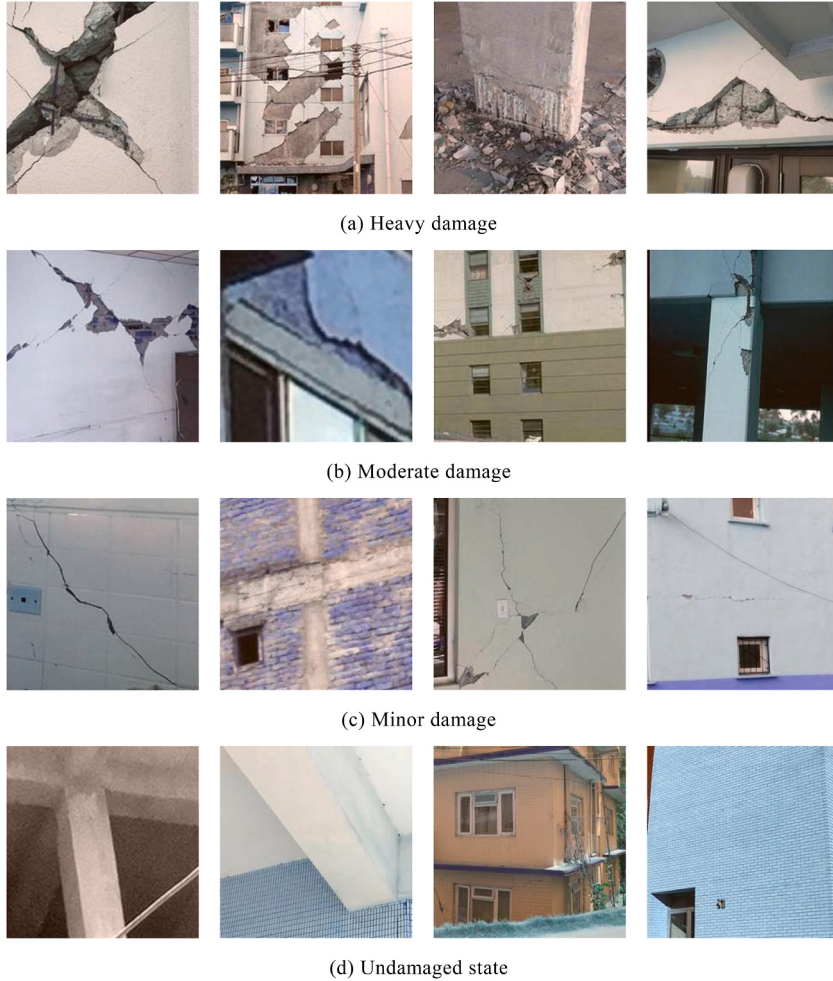


Fig. 3. Classification of damage level in ImageNet [31,42]. This image classification task contains a total of 4636 images, with 1013 for heavy damage, 903 for moderate damage, 962 for minor damage, 1758 for undamaged. Each category is randomly divided into training set, validation set, and test set in the ratio of 8:1:1.

horizontal loads to vertical members. Various components serve different functions, and it is essential to categorize them based on their functions for a comprehensive analysis.

φ -net [31,42] divides the structural members into four categories: beams, columns, walls, and others. Additionally, components beyond beams, columns, or walls are categorized as other structural elements, such as stairs, supports, and even non-structural elements including windows and doors. Joints play a crucial role in structures. However, as they are extensions of columns and beams, joints are often classified under the categories of “column” and “beam.” Therefore, a separate category for “Joints” is unnecessary. The greater the number of categories into which components are divided, the larger the amount of data required.

Therefore, it is reasonable to divide the component types into 4 categories: beam, column, wall, and others. Fig. 2 illustrates the classification of component type.

3.1.2. Task 2: component damage classification

Following an earthquake, various components of a building experience varying degrees of damage, each with distinct impacts on the overall structure. According to the code [40,41], building damage is categorized into five levels: essentially intact, minor damage, moderate damage, heavy damage, and collapse. The various levels of damage are detailed as follows: Essentially intact signifies that load-bearing components remain undamaged, some non-load-bearing components may incur slight damage, and auxiliary components exhibit varying degrees of damage, generally allowing continued use without repair. Minor damage involves minor cracks in individual load-bearing components, notable damage to individual non-load-bearing elements, and varying degrees of harm to ancillary components. These cases usually do not require repair or need only minimal maintenance to keep functionality. Moderate damage entails slight cracks in the majority of load-bearing elements, visible cracks in some areas, and substantial harm to specific non-load-bearing components. It necessitates general repairs and safe utilization through appropriate safety measures. Serious damage involves severe destruction or partial collapse of the majority of load-bearing components, demanding immediate emergency actions and significant reconstruction, including partial demolition where necessary. Collapse means that most load-bearing components collapse and need to be removed. Therefore, it is very important to identify the damage level of different components for the overall damage condition of the structure.

In φ -net [31,42], damage levels are defined into four categories: no damage, minor damage, moderate damage, and heavy damage. Minor damage is characterized by slight narrow cracks or a few spalling points on the surface of a structural member. Moderate damage signifies that, as the extent of damage intensifies, cracks widen, and additional spalling arises in areas that remain structurally sound. Heavy damage denotes extensive damage areas and imminent structural member failure. Whether significantly damaged or collapsed, the building poses severe safety risks and cannot be sustained. Since the focus is on the component level when determining the damage level, merging heavy damage and collapse as a single category at the component level is reasonable. Fig. 3 illustrates the classification of component type.

The dataset label distribution for the two classification tasks is shown in Fig. 4.

3.2. Deep learning network

3.2.1. EfficientNet architecture

Compared with traditional classification network structures, EfficientNet scales, combines, and optimizes three aspects: initial input image resolution, network structure depth, and width to obtain efficient collocation schemes, maximizing network performance when computing resources are fixed. The composite scaling model can focus on the regions related to more target details, and achieve the purpose of improving model accuracy and network performance while fully saving computing power resources. The computational principle of EfficientNet [24] can be represented by the following formula:

$$N(d, w, r) = \odot_{i=1 \dots s} F_i^{L_i}(X_{(H_i, W_i, C_i < >)}) \quad (1)$$

where, N represents the network model. d , w , and r represent the coefficients that scale the depth, width, and resolution of the network, respectively. $\odot_{i=1 \dots s}$ represents continuous multiplication. F represents network structure. L represents the number of layers, $F_i^{L_i}$ means that F has been repeated L_i times in stage i . X is the input feature matrix. H , W , C represent the height, width, and number of channels of

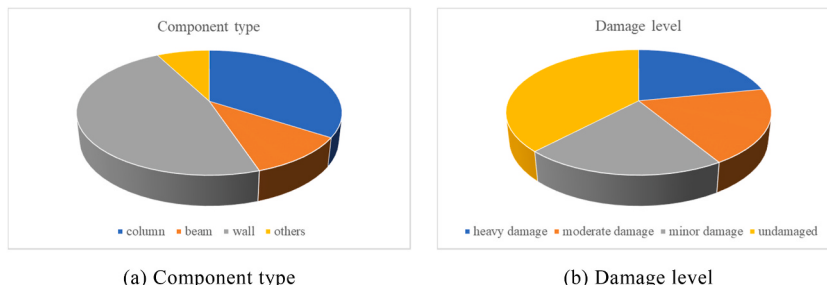


Fig. 4. Dataset label distribution for classification tasks.

\mathbf{X} , respectively. In order to explore the influence of d , w and r on the accuracy of the model under the given computing resources, the problem is abstracted as follows.

$$\underset{d,w,r}{\text{MaxAccuracy}}(N(d, w, r)) \quad (2)$$

$$\text{s.t } N(d, w, r) = \bigodot_{i=1 \dots s} \widehat{F}_i^{\widehat{L}_i}(X_{\langle r \cdot \widehat{H}_i, r \cdot \widehat{W}_i, \widehat{C}_i \rangle}) \quad (3)$$

$$\text{Memory}(N) \leq \text{target_memory} \quad (4)$$

$$\text{FLOPS}(N) \leq \text{target_flops} \quad (5)$$

where, Max Accuracy represents the maximum accuracy value of the network. s.t represents the restriction condition. $\widehat{F}_i^{\widehat{L}_i}$, \widehat{H}_i , \widehat{W}_i , \widehat{C}_i is the pre-set network structure and the height, width and number of channels of the input feature matrix \mathbf{X} . Memory represents the number of network parameters and target_memory represents the memory limit. FLOPS represents the number of floating-point operations and target_flops represents the limit of the number of floating-point operations. Based on these constraints and the network, a hybrid scaling method is proposed to uniformly adjust the depth, width and resolution of the network based on the hybrid factor ϕ . The calculation formula is as follows:

$$\text{depth : } d = \alpha^\phi \quad (6)$$

$$\text{width : } w = \beta^\phi \quad (7)$$

$$\text{resolution : } r = \gamma^\phi \quad (8)$$

$$\text{s.t. } \alpha \cdot \beta^2 \cdot \gamma^2 \approx 2 \quad (9)$$

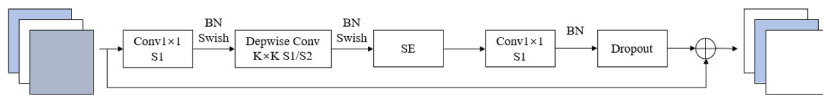
$$\alpha \geq 1, \beta \geq 1, \gamma \geq 1 \quad (10)$$

where, ϕ is the control coefficients set according to computer resources. The resource allocation coefficients of the depth, width, and resolution of the network corresponding to α , β , and γ are searched by Neural Architecture Search (NAS). The principle of NAS is to automatically test the combination of network structures by using some search strategy on the basis of the selected network, and obtain the best combination or parameter of network architecture after performance evaluation.

The core structure of EfficientNet is MBConv (Mobile inverted bottleneck convolution) module, which combines the attention mechanism of SENet (Squeeze and excitation network). Using the idea of MnasNet algorithm, the multi-objective deep neural architecture search operation is used to obtain the optimal parameters. The EfficientNet model is internally constituted by multiple MBConv convolution blocks, and the structure of a single MBConv block is shown in Fig. 5.

MBConv comprises 1×1 convolution for dimensionality expansion, $k \times k$ depthwise convolution, squeeze-and-excitation (SE) module, 1×1 convolution for dimensionality reduction, and a Dropout layer (see Fig. 6). In the MBConv module, the input image's feature information undergoes dimension expansion through convolution. The output channel dimension is adjusted based on the expansion ratio, and the feature information is then convolved with $k \times k$ depthwise to reduce the model's computational demands. Next, the adaptive attention operation persists through the squeeze and excitation module, enhancing the image feature information pertinent to the classification task. Subsequently, the feature information is reduced. Lastly, the random dropout layer executes random dropout operations, enhancing the model's capability to learn a robust feature representation and improve generalization [43]. The MBConv module incorporates a random depth feature, reducing model training time and enhancing overall performance.

SENet (Squeeze and excitation net) is a module employing channel attention mechanisms [44]. The SENet module within the MBConv convolution module is an attention-based feature map operation that emphasizes inter-channel correlations. It aims to enable the model to autonomously discern the importance of various channel features. Initially, the SENet module compresses the size of the



Note: Conv represents convolution, BN represents batch normalization, Swish represents the Swish activation function, Depwise represents depthwise convolution, SE represents squeeze and excitation, Dropout represents the random dropout layer, k represents the size of the convolution kernel, and $S1, S2$ represent the convolution kernel's stride.

Fig. 5. MBConv structure

Note : Conv represents convolution, BN represents batch normalization, Swish represents the Swish activation function, Depwise represents depthwise convolution, SE represents squeeze and excitation, Dropout represents the random dropout layer, k represents the size of the convolution kernel, and $S1, S2$ represent the convolution kernel's stride.

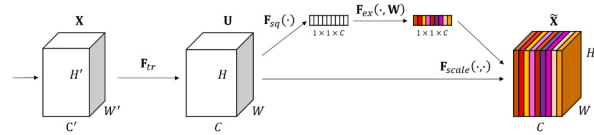


Fig. 6. Attention mechanism of SENet.

convolution-obtained feature map. It then conducts global average pooling on the feature map along the channel dimension, acquiring the global feature in the channel dimension. Subsequently, the excitation operation is performed on the global feature, that is, the global feature is multiplied by a 1×1 convolution in the number of the global feature dimension with the activation ratio. This process aims to learn the relationships between each channel. The fully connected network is employed to derive the weight of each channel through the Sigmoid activation function transformation. Finally, it is multiplied with the original feature map to produce the ultimate output feature. The SENet module performs attention or gate control operations on the channel dimension, enabling the model to focus more on channel features containing crucial information and suppress less important ones.

In this paper, the parameter size of the network and the model performance are comprehensively considered, and the EfficientNetB3 network is selected for transfer learning. The network structure of the EfficientNetB3 is as follows (Table 1):

3.2.2. Network optimization design

Training CNN models with numerous layers and parameters from scratch can be highly challenging. Simultaneously, training deep networks typically demands an extensive dataset, which can pose challenges for users with limited computing resources. Transfer learning [31] is an ML technique that applies knowledge transfer from one domain (the source domain) to another (the target domain) to enhance learning outcomes in the target domain. This enables the reuse of a pre-trained convolutional neural network on a specific dataset and the adaptation or transfer of the network to other datasets.

Deep learning frameworks provide a fast way to build target models through preconstructed parts. In order to improve the efficiency of code construction for new projects, some researchers encapsulate the repetitive base code into different frameworks through their respective computer languages. Deep learning framework allows users to build deep learning models more quickly and easily without in-depth knowledge of the basic algorithm details, which is of great significance for the application and promotion of deep learning across disciplines. PyTorch is a popular deep learning framework that is widely adopted by the academic community. PyTorch is a dynamic framework that continuously inputs data during the construction of each layer of the model, then observes the output of each layer of the neural network, and modifies the model in real time. PyTorch offers access to prevalent deep learning networks through the use of ImageNet datasets and pre-trained models, which can be fine-tuned to meet specific requirements, expediting task completion.

In a neural network model, the loss function is a quantitative expression of the difference between the probabilistic model in the network and the ideal probabilistic model. In this paper, the cross entropy loss function is selected, and the expression is as follows:

$$H(X) = - \sum_{i=1}^n P(x_i) \log(Q(x_i)) \quad (X = x_1, x_2, x_3, \dots, x_n) \quad (11)$$

where, $P(x_i)$ represents the true value, $Q(x_i)$ represents the calculated softmax value.

The stochastic gradient descent (SGD) algorithm is an effective optimization method. Typically, the objective function is stochastic, and a subset of data is used for the gradient descent operation to find the optimal solution. In each iteration, the following formula can be used for the update of parameter θ :

$$\theta_{t+1} = \theta_t - \alpha \nabla J(\theta_t; x^{(i)}, y^{(i)}) \quad (12)$$

where, θ_t is the model parameter in iteration t times. α is the learning rate. $J(\theta_t; x^{(i)}, y^{(i)})$ is a loss function that represents the difference between the model's prediction on the input $x^{(i)}$ and the actual label $y^{(i)}$. $\nabla J(\theta_t; x^{(i)}, y^{(i)})$ is the gradient of the loss function to the model parameters.

Table 1
The network structure of the EfficientNetB3.

Stage	Operator	Channels	Layers
1	Conv 3×3	40	1
2	MBConv1, $k3 \times 3$	24	2
3	MBConv6, $k3 \times 3$	32	3
4	MBConv6, $k5 \times 5$	48	3
5	MBConv6, $k3 \times 3$	96	5
6	MBConv6, $k5 \times 5$	136	5
7	MBConv6, $k5 \times 5$	232	6
8	MBConv6, $k3 \times 3$	384	2
9	Conv 1×1 &Pooling&FC	1536	1

When training deep learning models, SGD with momentum and L2 regularization can help improve the model's generalization ability, prevent overfitting, and accelerate the model's convergence on the training data. Momentum updates the parameters in the network by simulating the inertia of the object motion, that is, the direction of the previous parameter update is considered to a certain extent when updating. At the same time, the gradient calculated by the current batch is used to combine the direction to calculate the size and direction of the parameter update. Using momentum not only increases the stability of the learned parameters to a certain extent, but also will learn the converged parameters faster. Regularization usually adds a penalty norm on the training parameters to the loss function, and the parameters that need to be trained are constrained by the added norm penalty to prevent the model from overfitting. The L2 -norm penalty term aims to minimize the sum of the squares of the parameters. Using the L2 norm for the constraint will select more parameters, but these parameters will be close to 0 to prevent the model from overfitting. SGD with momentum and L2 regularization in deep learning can be obtained by adding momentum terms and L2 regularization terms to standard SGD update rules. In each iteration, the following formula can be used for the update of parameter θ :

$$\nu_{t+1} = \beta\nu_t + (1 - \beta)\nabla J(\theta_t; \mathbf{x}^{(i)}, \mathbf{y}^{(i)}) - \lambda\alpha\theta_t \quad (13)$$

$$\theta_{t+1} = \theta_t - \alpha\nu_{t+1} \quad (14)$$

where, ν_t is the momentum term, representing the momentum in iteration t times. β is the attenuation coefficient of momentum, usually between [0,1]. λ is a hyperparameter of L2 regularization. The L2 regularization term $-\lambda\alpha\theta_t$ is added to the momentum update, where λ controls the intensity of the regularization.

3.2.3. Hyperparameter setting

From a preliminary convergence analysis, these are set to 80 training epochs for component type classification and 120 training epochs for damage level classification, 32 batch sizes, and the accuracy is calculated at the end of each training epoch. Resizedcrop and horizontal flip operations are employed for data augmentation. To prevent confusion between "column" and "beam" caused by rotation, rotation is excluded from the data augmentation process. The attenuation learning rate is selected for training optimization. Regarding the attenuation strategy of learning rate, a large learning rate helps to avoid the model falling into a local minimum in the early stages of training, and a certain degree of exploration is expected from the model. After early training, the learning rate is reduced, and such a small learning rate stabilizes the model and avoids large shocks. The initial learning rate is set to 0.01, momentum is set to 0.9, and weight decay is set to 0.0004. The accuracy and loss histories are shown in Fig. 7.

3.2.4. Performance evaluation of the models

For classification problems, the performance evaluation indicators of the prediction model are generally accuracy, precision, recall, F1-score, confusion matrix, etc. Accuracy represents the proportion of samples with correct classification in all samples; precision

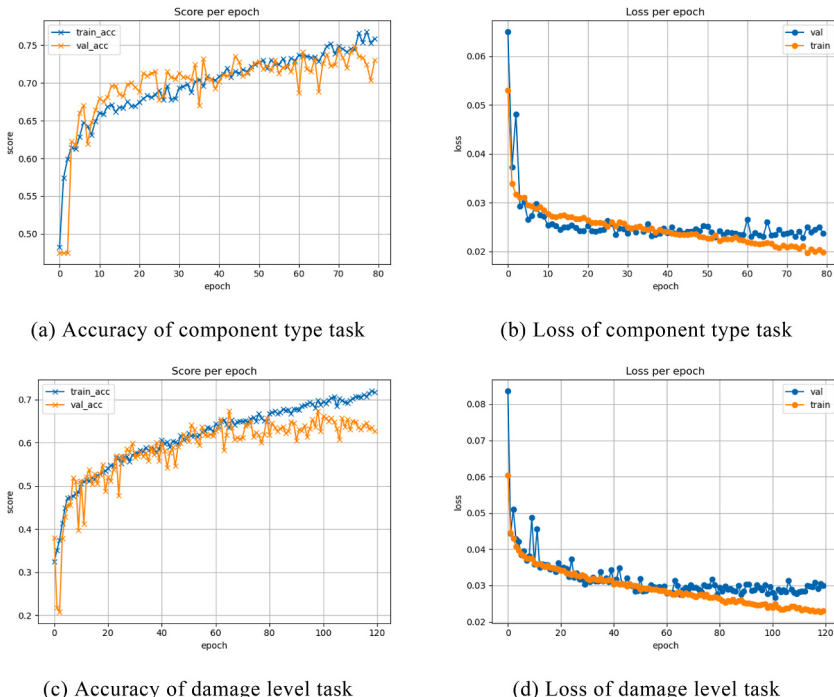


Fig. 7. Accuracy and loss histories.

represents the proportion of a sample classified as positive; recall represents the probability that a sample is predicted to be positive in a sample that is actually positive. The confusion matrix visually shows the relationship between the true and predicted values. In particular, the diagonal elements of the confusion matrix represent the number of samples correctly predicted, while the off-diagonal elements represent the number of samples incorrectly classified. The formula of each evaluation indicator is as follows.

$$\text{Accuracy} = \frac{TP + TN}{TP + FP + FN + TN} \quad (15)$$

$$\text{Precision} = \frac{TP}{TP + FP} \quad (16)$$

$$\text{Recall} = \frac{TP}{TP + FN} \quad (17)$$

$$F1\text{-score} = \frac{2\text{Precision} * \text{Recall}}{\text{Precision} + \text{Recall}} \quad (18)$$

where, TP (True Positive) represents the number of positive samples classified as positive samples by the model, and TN (True Negative) represents the number of negative samples classified as negative samples by the model. FP (False Positive) represents the number of negative samples classified by the model as positive samples, and FN (False Negative) represents the number of positive samples classified as negative samples.

The confusion matrix predicted on the test set is shown in Fig. 8.

For the two classification tasks of component type and damage level, the final classification accuracy can be obtained based on Equation (15) and Fig. 8.

The accuracy of the component type classification task:

$$\text{Accuracy} = \frac{156 + 45 + 180 + 8}{156 + 0 + 20 + 6 + 2 + 45 + 7 + 3 + 49 + 17 + 180 + 7 + 15 + 3 + 15 + 8} = \frac{389}{533} = 0.7289 \quad (19)$$

The accuracy of the damage level classification task:

$$\text{Accuracy} = \frac{64 + 34 + 54 + 138}{64 + 21 + 6 + 10 + 15 + 34 + 22 + 19 + 2 + 11 + 54 + 29 + 9 + 11 + 18 + 138} = \frac{290}{463} = 0.6263 \quad (20)$$

Therefore, the classification accuracy rates for the component type and damage level are 72.89 % and 62.63 %, respectively.

According to the definitions of precision and recall above, precision evaluates the model's ability to make precise and reliable positive predictions, while recall assesses the model's ability to capture all positive instances in the dataset. The F1-score, taking both precision and recall into account, represents the harmonic mean of the two metrics.

As shown in Table 2, in the task of component type classification, columns, beams, and walls can be more accurately distinguished, while the evaluation metrics of the type of "others" are relatively low. Although the score is low in numerical terms, considering that "others" refer to joints, stairs, supports, and even non-structural elements such as windows and doors, these components usually play a less important role in structural function than columns, beams, and walls, so it is more conservative and safer to classify "others" as other labels.

As shown in Table 3, In the task of damage level classification, heavy damage and undamaged state can be accurately classified, while the evaluation metrics of the type of moderate damage and minor damage are relatively low. The reason for this problem may be

		Predicted label				
		Column	Beam	Wall	Others	
True label	Column	156	0	20	6	182
	Beam	2	45	7	3	57
	Wall	49	17	180	7	253
	Others	15	3	15	8	41
		222	65	222	24	533

		Predicted label				
		Heavy	Moderate	Minor	Undamaged	
True label	Heavy	64	21	6	10	101
	Moderate	15	34	22	19	90
	Minor	2	11	54	29	96
	Undamaged	9	11	18	138	176
		90	77	100	196	463

(a) Component type

(b) Damage level

Fig. 8. Confusion matrices of two classification tasks.

Table 2

Performance measures for component type classification model on test set.

Measure	Precision	Recall	F1-score
Column	0.70	0.86	0.77
Beam	0.69	0.79	0.74
Wall	0.81	0.71	0.76
Others	0.33	0.20	0.25

the relatively small dataset and some engineering subjectivity and ambiguity on how to judge minor damage versus moderate damage. Assigning a certain damage level from two adjacent levels usually a nebulous work. Therefore, the machine learning model is actually learning tags with original uncertainty. The error here is also acceptable.

In Fig. 7, the optimal accuracy of the two classification tasks of component type and damage level in the validation set is 74.90 % and 67.40 %, and the model with the best effect is saved, which is used as the model for the subsequent classification of component type and damage level. The classification tasks of component type and damage level are four classification tasks. Even though there are overfitting problems in the classification tasks, compared with the expected accuracies of 25.0 % from random guesses of four-classes classification problem, the obtained 74.90 % and 67.40 % are higher than expected. Upon reviewing recent literature, it has been noted that the accuracy of the classification of component type and damage level matches the findings of this paper [31,42,45]. The overall structure comprises numerous component types. Accurately distinguishing component types is indeed complex due to factors such as different image shooting angles and extraneous objects in the same image. As for damage level, accurately distinguishing damage severity for each level proves challenging due to the intricate presentation of damage degrees.

4. Structural-level damage assessment using components integration

4.1. Structural-level damage definition

To calculate the overall condition of the structure based on the number of component types and damage levels, varying weights should be assigned to distinct component types and damage levels. Both the weight definition of component type and damage level will impact the ultimate result. Considering relevant engineering regulations and experience, the fundamental weight allocation principles are as follows: in terms of component types, the weight of load-bearing components is greater than that of non-load-bearing components, and the weight of vertical load-bearing components is greater than that of horizontal load-bearing components. In terms of damage level, the more severe the damage, the higher the weight.

The Chinese code for maintenance of highway bridges [46] established a specific operational process for assessing the condition of bridges. Considering bridge specifications and practical application scenarios, Feng et al. [47] proposed a detailed condition rating rule for bridges. In the method proposed by Feng et al. the weight of each bridge component is assigned based on its importance, and the corresponding score is made according to the condition of the damage and the development of the damage. Eventually, the scores of individual components are aggregated using the weighted formula. Table 4 can be obtained by classifying and summing the parts of bridge.

Most civil engineering buildings are low-rise reinforced concrete frame structures and brick-concrete structures. In a structural system, different structural components play different roles. In accordance with mechanical principles, greater weight is allocated to the more critical components of the system. Based on engineering theory and practical experience, columns carry both vertical and lateral loads, while beams primarily carry vertical loads. Therefore, columns and beams are assigned higher weights. Walls in concrete structures might either act as load-bearing elements or solely contribute to space division. Taking into account both of them, when assigning component weights, the weight assigned to walls is lower than that assigned to beams. As a result, the preliminary order of component type weights can be determined as follows: columns, beams, walls, and others, ranging from high to low. The weight values attributed to various components in concrete construction are detailed in Table 5. The weight values for various damage levels are detailed in Table 6.

Based on the classification results of a building by component type and damage level, the scores of each component are weighted and summed. The final score is based on a deduction system, with a maximum score of 100 points. A lower score indicates more severe damage.

Table 3

Performance measures for damage level classification model on test set.

Measure	Precision	Recall	F1-score
Heavy damage	0.71	0.63	0.67
Moderate damage	0.44	0.38	0.41
Minor damage	0.54	0.56	0.55
Undamaged state	0.70	0.78	0.74

Table 4
The weight of each part of bridge.

Parts	Weight of part
Deck system	14
Superstructure	25
Substructure	47
Ancillary facilities	14

Table 5
Weight of component type in concrete structure.

Type of component	Weight of component type
Column	45
Beam	25
Wall	20
Others	10

Table 6
Weight of component damage level in concrete structure.

Level of damage	Weight of damage level
Heavy damage	3
Moderate damage	2
Minor damage	1
Undamaged state	0

4.2. Structural-level damage calculation procedure

In practical application, the evaluation method of structural-level damage proposed in this paper consists of four main steps: image acquisition and preprocessing, image classification, statistical analysis of classification results, and prediction and assessment of the overall condition level of the structure.

4.2.1. Image data acquisition and preprocessing

To collect images of components of post-earthquake buildings requiring evaluation, tools that can take images such as drones and smartphones can be employed. Organize images from the same building into the same folder. To ensure accuracy, it is essential to collect images of damaged building components comprehensively, so that the collected images cover most areas of the building, damage and different components to the fullest extent. It's advisable to gather a substantial number of images overall, ideally having no less than 50 images per building. In addition, the images with significant interference or poor quality can be manually excluded.

	Column	Beam	Wall	Others	
Heavy damage	n_{11}	n_{12}	n_{13}	n_{14}	n_{10}
Moderate damage	n_{21}	n_{22}	n_{23}	n_{24}	n_{20}
Minor damage	n_{31}	n_{32}	n_{33}	n_{34}	n_{30}
Undamaged	n_{41}	n_{42}	n_{43}	n_{44}	n_{40}
	n_{01}	n_{02}	n_{03}	n_{04}	N

Fig. 9. Statistical chart of prediction results.

Note that the first principle about data acquisition is that we need to capture the images for all the components as possible as we can, since the following integration is performed on different components. This will ensure that we won't lose any damage information about the building. For some technique reasons, one will take multiple images for some components, but the final classification results for each component should the average of all the images to reduce the model uncertainty.

4.2.2. Structural-level damage integration rules

The images collected from the same building are fed into the pre-trained models for component type classification and damage level classification. This process yields classification results for the component types and damage levels of the building's component images.

Based on the output results of component classification model and damage level classification model, the number of each classification result is counted. Following the structure of a confusion matrix, the statistical approach adopted in this study utilizes the component types (column, beam, wall, and others) as the horizontal axis and the damage levels (heavy damage, moderate damage, minor damage, and undamaged) as the vertical axis. The detailed form is illustrated in Fig. 9.

The data in Fig. 9 has the following quantitative relationship.

$$N = n_{01} + n_{02} + n_{03} + n_{04} = n_{10} + n_{20} + n_{30} + n_{40} \quad (21)$$

$$n_{0j} = \sum_{i=1}^4 n_{ij} (j = 1, 2, 3, 4) \quad (22)$$

$$n_{i0} = \sum_{j=1}^4 n_{ij} (i = 1, 2, 3, 4) \quad (23)$$

where n_{ij} represents the number of images under the corresponding situation.

In comprehensively consider and intuitively represent the damage level of identical component within a single building, this paper introduces the concept of the weighted damage level for components. For the same component type, if there are n_1 of heavy damage, n_2 of moderate damage, n_3 of minor damage, and n_4 of undamaged state, the weighted damage level of the component is calculated as:

$$R_i = \frac{3 \times n_1 + 2 \times n_2 + 1 \times n_3 + 0 \times n_4}{n_1 + n_2 + n_3 + n_4} \quad (24)$$

Taking the column as an example, the weighted damage level is calculated by formula (10).

$$R_c = \frac{3 \times n_{11} + 2 \times n_{21} + 1 \times n_{31} + 0 \times n_{41}}{n_{11} + n_{21} + n_{31} + n_{41}} = \frac{3 \times n_{11} + 2 \times n_{21} + 1 \times n_{31}}{n_{01}} \quad (25)$$

In practical application, the weighting calculation formula is as follows:

$$score = 100 - \sum_{i=1}^n \frac{R_i W_i}{3} \quad (26)$$

where:

$score$ —The structure overall condition score

n —The number of component types

R_i —The weighted damage level of the same component of the same building

W_i —The weight of corresponding component type

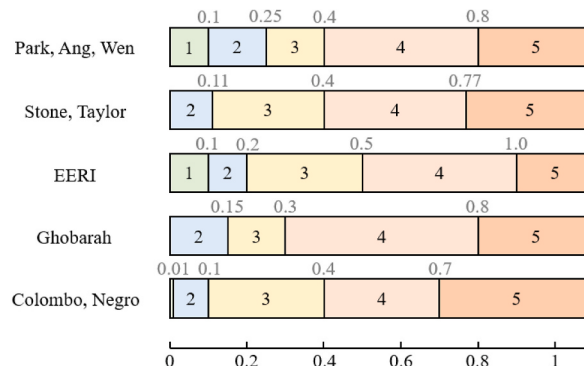


Fig. 10. Summary of structural damage index.

The formula yields the overall condition score for the entire structure, making assessment from individual components to the entire structure. The damage level of the entire structure is determined based on the overall condition score and classification limit scores. The overall condition level ranges from level 1 to level 5, signifying worsening condition. If the current building's overall condition is assessed as poor, it is advisable to prioritize the allocation of personnel and funds, conduct timely and thorough inspection and maintenance, aiming to mitigate losses from delayed damage detection.

However, there is no uniform standard for structural damage score and structural damage level. Bai et al. sorted out several authority correspondence relations between structural damage index and structural damage level [48–52], as illustrated in Fig. 10.

Using the summary chart and the evaluation method proposed in this paper, the damage index can be transformed into a 100-point scale score, facilitating assessment of the overall structural condition level. Taking Park, Ang, Wen standard as an example, the corresponding 100-point scores of each level are listed in Table 7. Other criteria can be obtained in the same way.

5. Application case study

5.1. Dataset collection and description

At 22:55 on June 17, 2019, an earthquake with a magnitude of 6.0 struck Changning County, Yibin City, Sichuan Province, China at a depth of 16 km. The 5.4-magnitude earthquake that occurred in Gongxian County at 22:29 on June 22, 2019 was an aftershock of the 6.0-magnitude Changning earthquake on June 17. Preliminary verification statistics indicate varying degrees of damage to power, communications, water supply, gas supply, transportation facilities, and the ecological environment in the earthquake-stricken area. As a result, 20,185 houses belonging to 9532 households have either collapsed or suffered significant damage.

After the earthquake, the relevant inspectors from Sichuan Institute of Building Research used manual photography to collect images of 23 buildings from Gongxian County, which were mainly distributed on both sides of Mishi Street. Each building has different numbers of components and different numbers of images, but overall, the images nearly cover all the components for the building. The images were labeled by professional experts to denote the component type and damage levels. To show the efficiency of the proposed method, the seismic damage images of 23 houses situated in Gongxian County are analyzed.

5.2. Results for component images

Firstly, the image classification results of a single image in a single building can be compared with the actual image content to check the accuracy of the image classification prediction results. Here we take the images from the building at No.74 Mishi Street in Gongxian County as an example. A total of 125 images of the building are collected. These images are input into both the component type classification model and the damage level classification model, resulting in corresponding classification outcomes. From these pictures, the type and damage level of each component in every image can be accurately determined. The overall accuracy is around 0.75 since this case has sufficient images. Typical images of the building are shown in Fig. 11. Fig. 11(a) displays the predicted result of moderate damage to the wall. The image shows a large-scale peeling of the protective layer on the wall, aligning accurately with the prediction. Fig. 11(b) displays the predicted result of an undamaged state for the column. The image shows that the column has only slight cracks on the protective layer. Fig. 11(c) displays the predicted result of an undamaged state for the beam. The image shows that there is no damage to the beam. Fig. 11(d) displays the predicted result of moderate damage to the wall. The image shows large-scale cracks spreading throughout the wall, aligning with the prediction of moderate damage. Fig. 11(e) displays the predicted result of an undamaged state for other components. The image shows the location where the concrete staircase meets the wall, and there is no damage observed. Fig. 11(f) displays the predicted result of minor damage to the wall. The image shows a diagonal crack in the wall, consistent with the prediction of minor damage. In summary, the outcomes of image classification align closely with the real conditions, so it can provide accurate component hierarchy type information and damage level information for the overall condition score.

5.3. Results of typical buildings

Summing up all the outcomes of the components yields the results for each building. Still take the building at No.74 Mishi Street in Gongxian County as an example, the final results for all the component images are shown in Fig. 12.

Based on Eq. (22), the weighted damage level of each component can be calculated as follows:

Weighted damage level of column:

Table 7

The 100-point scale scores corresponding to the structural damage index proposed by Park, Ang, Wen.

Structural damage index	Corresponding 100-point scale scores	Structural damage level
0–0.1	score \geq 90	1
0.1–0.25	75 \leq score $<$ 90	2
0.25–0.4	60 \leq score $<$ 75	3
0.4–0.8	20 \leq score $<$ 60	4
>0.8	score $<$ 20	5



Fig. 11. Typical images of the building, situated at No. 74 Mishi Street, Gongxian County.

	Column	Beam	Wall	Others
Heavy damage	1	0	4	0
Moderate damage	2	0	14	0
Minor damage	4	5	42	0
Undamaged	1	6	45	1
	8	11	105	1
				125

Fig. 12. Statistics of image prediction results of the building, situated at No. 74 Mishi Street, Gongxian County.

$$\frac{1}{8} \times 0 + \frac{4}{8} \times 1 + \frac{2}{8} \times 2 + \frac{1}{8} \times 3 = 1.375 \quad (27)$$

Weighted damage level of beam:

$$\frac{6}{11} \times 0 + \frac{5}{11} \times 1 = 0.455 \quad (28)$$

Weighted damage level of wall:

$$\frac{45}{105} \times 0 + \frac{42}{105} \times 1 + \frac{14}{105} \times 2 + \frac{4}{105} \times 3 = 0.781 \quad (29)$$

Weighted damage level of others:

$$\frac{1}{1} \times 0 = 0 \quad (30)$$

Integrating the weights of component type and damage level with the calculation formula outlined in Section 4 [Eq. (26)] yields the final overall condition score of the building, which is 70.377, say,

$$score = 100 - \frac{45 \times 1.375 + 25 \times 0.455 + 20 \times 0.781 + 10 \times 0}{3} = 70.377 \quad (31)$$

Two other typical buildings are also selected for detailed discussion. To comprehensively cover the score distribution, we select buildings with scores around 70, 80, and 90, representing varying damage conditions. The calculated scores for the typical buildings are presented in Fig. 13. Fig. 13(a) depicts a building with a slightly peeled-off facade and some walls exhibiting minor cracks while other components remain intact. The damage condition aligns relatively well with the calculated score. Fig. 13(b) illustrates walls with large-scale peeling, wide and long cracks, and some beams showing cracks. Therefore, a score just above 70 is a relatively accurate representation of its condition. Fig. 13(c) shows walls with slight cracks, and some walls have large, extensive cracks, while other components remain mostly intact. Consequently, a score below 80 accurately indicates its condition. In summary, the analysis of three typical cases reveals a relatively high degree of alignment between the calculated score and the actual earthquake damage, providing valuable support for subsequent decision-making.

According to the condition classification limit score, the condition level of the building can be categorized into level three. This indicates that the condition of the building is relatively poor, and corresponding response measures should be taken immediately to avoid losses caused by not timely detection.

With reference to the standards of Park, Ang, and Wen, the condition level distribution of the buildings collected after the earthquake in Gongxian County is shown in Table 8 and classification result distribution is shown in Fig. 14 (see Table 9).

The tables (Table 9, 10, 11 and 12) below display the outcomes of alternative classification criteria. The distribution of classification results based on different criteria are shown in Fig. 15.

Fig. 15 reveals variations in the classification of the overall structural condition based on different criteria. In practical engineering applications, there is flexibility in selecting criteria that align with specific circumstances. While the selection is subjective, it is advisable to choose criteria that can distinguish more levels for better differentiation of the building's damage level. This facilitates the identification of priority targets for immediate action in subsequent maintenance efforts, efficiently pinpointing the most severely damaged buildings. For instance, in the case of this paper, the structural damage index proposed by Park, Ang, Wen, and EERI is a preferable choice as it allows for the distinction of more levels compared to other criteria.

Additionally, it's important to give adequate consideration to buildings with intermediate scores. Since this method solely accounts for the building's internal damage, practical building damage assessments should also consider the influence of external environmental factors.



Fig. 13. Prediction scores for typical buildings.

Table 8
Classification results based on Park, Ang, Wen.

Classification level	Quantity
1	7
2	13
3	3
4	0
5	0

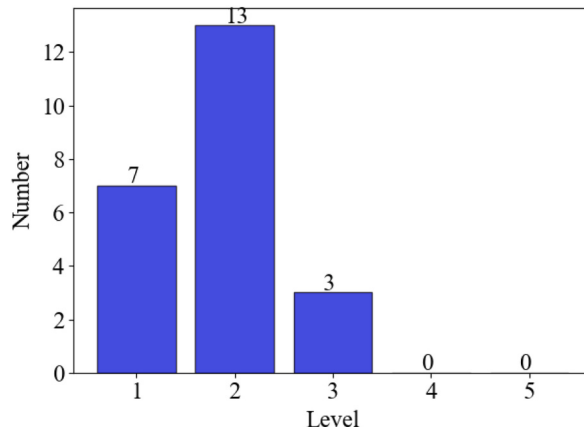


Fig. 14. Classification result distribution based on Park, Ang, Wen.

Table 9
Classification results based on Stone, Taylor.

Classification level	Corresponding 100-point scale scores	Quantity
1	score = 100	0
2	89 ≤ score < 100	8
3	60 ≤ score < 89	15
4	23 ≤ score < 60	0
5	score < 23	0

Table 10
Classification results based on EERI.

Classification level	Corresponding 100-point scale scores	Quantity
1	score ≥ 90	7
2	80 ≤ score < 90	11
3	50 ≤ score < 80	5
4	10 ≤ score < 50	0
5	score < 10	0

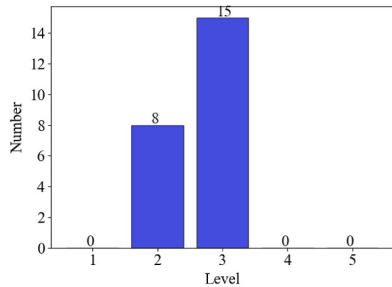
Table 11
Classification results based on Ghobarah.

Classification level	Corresponding 100-point scale scores	Quantity
1	score = 100	0
2	85 ≤ score < 100	12
3	70 ≤ score < 85	11
4	20 ≤ score < 70	0
5	score < 20	0

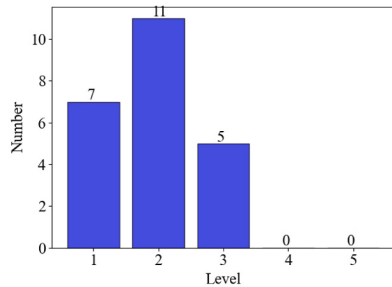
Table 12

Classification results based on Colombo, Negro.

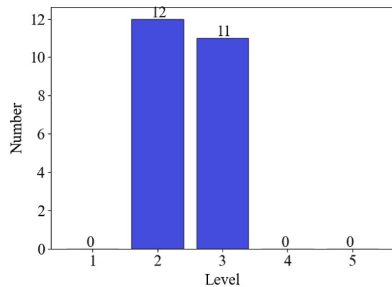
Classification level	Corresponding 100-point scale scores	Quantity
1	score ≥ 99	0
2	$90 \leq \text{score} < 99$	7
3	$60 \leq \text{score} < 90$	16
4	$30 \leq \text{score} < 60$	0
5	score < 30	0



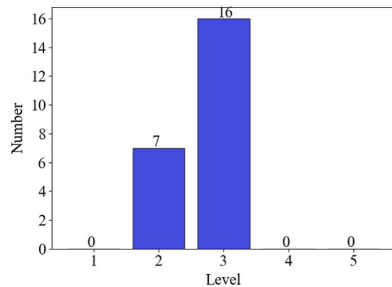
(a) Based on Stone and Taylor



(b) Based on EERI



(c) Based on Ghobarah



(d) Based on Colombo and Negro

Fig. 15. Distribution of classification results.**Table 13**

The overall condition scores of buildings after the earthquake in Gongxian County.

Number	Score	Number	Score
1	88.375	2	71.193
3	87.083	4	82.530
5	81.963	6	85.750
7	90.000	8	83.460
9	98.333	10	70.377
11	92.780	12	92.612
13	91.500	14	91.547
15	86.333	16	79.600
17	83.328	18	71.667
19	80.035	20	79.000
21	80.000	22	89.038
23	96.667		

5.4. Results across all building portfolios

Based on the structural-level damage evaluation procedure outlined in Section 4.2, 23 houses located in Gongxian County can be evaluated. Each house gets a score based on the collected images. The overall condition scores of buildings after the earthquake in Gongxian County are shown in Table 13. The distribution of condition scores across all building portfolios is shown in Fig. 16. From the tabulated data and the data distribution diagram, it can be seen that the overall building condition scores range from 70 to 100, which is numerically distinguishable. The calculated scores indicate that there are 7 houses with scores above 90, 5 houses with scores

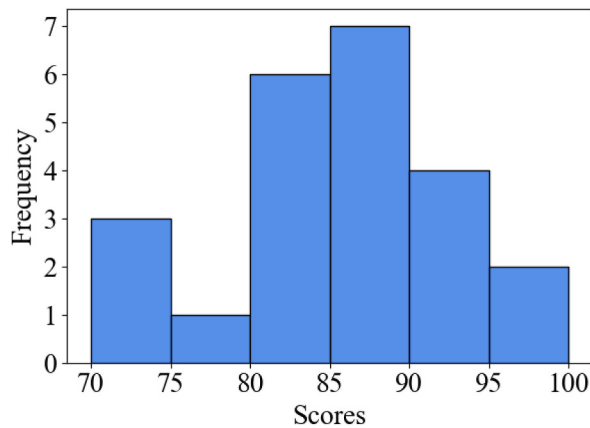


Fig. 16. The distribution of condition score across all building portfolios.

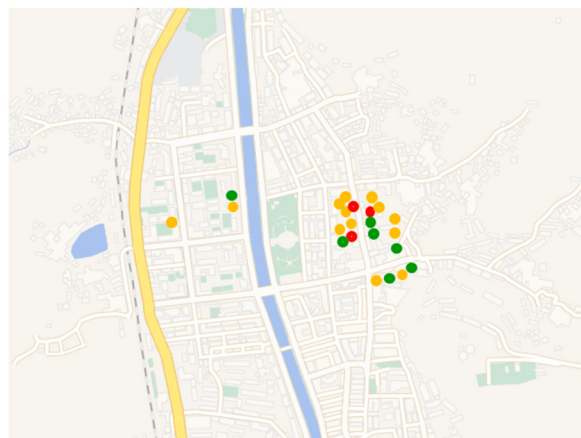


Fig. 17. Spatial distribution of damaged buildings based on Park, Ang, Wen.

between 85 and 90, 6 houses with scores between 80 and 85, and 5 houses with scores between 70 and 80. The spatial distribution of damaged buildings, based on Park, Ang, and Wen, is illustrated in Fig. 17. The spatial distribution map uses green to represent structures with a damage level of 1, yellow for a damage level of 2, red for a damage level of 3, and there are no houses with damage levels 4 and 5. This approach allows for the swift acquisition of post-earthquake building damage conditions, providing support for subsequent decision-making.

6. Conclusions

This paper proposed a rapid assessment method for determining the overall damage level of post-earthquake buildings using component images and DL. By collecting the component images of post-earthquake buildings, the component types and damage levels were classified based on EfficientNet and transfer learning. Based on the image classification results and the weight of the corresponding category, the overall score of the structure can be calculated by weighting, which realizes the expansion from the component level to the structure level and grasps the condition of the structure from the global scale. The score calculated by the formula proposed in the paper can correspond to the condition of the image, highlighting the validity of the assessment approach introduced in this paper. This method holds significant importance in guiding the evaluation of post-earthquake building overall condition, directing subsequent resource allocation, and formulating maintenance responses.

It is worth noting that the method proposed in this paper also has some limitations. In terms of image collection, it is necessary to collect a substantial quantity of images, but also need to cover a wide range of aspects of the structure, and the quality of images needs to be ensured. Each time before evaluating a building, image collection is of great necessity. If the images collected on the buildings to be evaluated are insufficient, or some images of poor quality are used, the calculated score will be affected, thus affecting the subsequent judgment. This paper does not make a strict distinction between structure types. While the paper validates the approach using actual earthquake data, the long-term durability would require continuous updating and retraining of models as new data becomes available.

The future work should address the scalability of the method and its applicability to different types of buildings and seismic events. The future research direction mainly includes the following aspects. Firstly, the dataset should ideally cover a wide range of building types, component types, and damage levels to ensure the model's robustness and applicability to various real-world scenarios. Secondly, in the classification of component type, interested researchers can subdivide more component types in the "others" category to enhance the precision of component identification. Thirdly, future studies may try to set the weight of component types as an interval, and fully explore the influence of weight distribution of different component types on the overall condition score.

CRediT authorship contribution statement

De-Cheng Feng: Writing – review & editing, Supervision, Project administration, Investigation, Funding acquisition, Formal analysis, Conceptualization. **Xin Yi:** Writing – original draft, Formal analysis, Data curation. **Zeynep Tuna Deger:** Writing – review & editing, Resources. **Han-kun Liu:** Resources, Funding acquisition. **Shi-Zhi Chen:** Writing – review & editing, Supervision, Resources, Conceptualization. **Gang Wu:** Supervision.

Declaration of competing interest

The authors declare that they have no known competing financial interests or personal relationships that could have appeared to influence the work reported in this paper.

Acknowledgments

The first author greatly appreciates the financial supports from the Project of National Key Research and Development Program of China (Grant No. 2022YFC3803000), the National Natural Science Foundation of China (Grant No. 52361135806), and the Fundamental Research Funds for the Central Universities (Grant No. 2242024K40012).

Data availability

Data will be made available on request.

References

- [1] E.D. Alexandra Moshou, Panagiotis Argyrakis, A Review of the November 26th 2019 Durres, Albania Earthquake Mw, 6.4, 2019.
- [2] J. Atalić, M. Demšić, M. Banicek, M. Uroš, I. Dasović, S. Prevolnik, A. Kadić, M. Savor Novak, M. Nastev, The December 2020 magnitude (Mw) 6.4 Petrinja earthquake, Croatia: seismological aspects, emergency response and impacts, *Bull. Earthq. Eng.* 21 (13) (2023) 5767–5808.
- [3] W. Chen, G. Rao, D. Kang, Z. Wan, D. Wang, Early report of the source characteristics, ground motions, and casualty estimates of the 2023 Mw 7.8 and 7.5 Turkey earthquakes, *J. Earth Sci.* 34 (2) (2023) 297–303.
- [4] Chen, T., and Guestrin, C. "Xgboost: a scalable tree boosting system." Proc., Proceedings of the 22nd ACM SIGKDD International Conference on Knowledge Discovery and Data Mining, 785-794.
- [5] D.C. Feng, Z.T. Liu, X.D. Wang, Y. Chen, J.Q. Chang, D.F. Wei, Z.M. Jiang, Machine learning-based compressive strength prediction for concrete: an adaptive boosting approach, *Construct. Build. Mater.* 230 (2020).
- [6] Y. Freund, R.E. Schapire, A decision-theoretic generalization of on-line learning and an application to boosting, *J. Comput. Syst. Sci.* 55 (1) (1997) 119–139.
- [7] M.H. Hassoun, Fundamentals of Artificial Neural Networks, MIT press, 1995.
- [8] M.A. Hearst, S.T. Dumais, E. Osuna, J. Platt, B. Scholkopf, Support vector machines, *IEEE Trans. Pattern Anal. Mach. Intell.* 20 (1) (1998) 18–28.
- [9] S. Mangalathu, H.V. Burton, Deep learning-based classification of earthquake-impacted buildings using textual damage descriptions, *Int. J. Disaster Risk Reduc.* 36 (2019).
- [10] S.R. Safavian, D. Landgrebe, A survey of decision tree classifier methodology, *IEEE transactions on systems, man, and cybernetics* 21 (3) (1991) 660–674.
- [11] H. Sun, H.V. Burton, H.L. Huang, Machine learning applications for building structural design and performance assessment: state-of-the-art review, *J. Build. Eng.* 33 (2021).
- [12] Y. LeCun, Y. Bengio, G. Hinton, Deep learning, *Nature* 521 (7553) (2015) 436–444.
- [13] Y. LeCun, L. Bottou, Y. Bengio, P. Haffner, Gradient-based learning applied to document recognition, *Proc. IEEE* 86 (11) (1998) 2278–2324.
- [14] A. Krizhevsky, I. Sutskever, G.E. Hinton, Imagenet classification with deep convolutional neural networks, *Adv. Neural Inf. Process. Syst.* 25 (2012).
- [15] K. Simonyan, A. Zisserman, Very Deep Convolutional Networks for Large-Scale Image Recognition, 2014 *arXiv preprint arXiv:1409.1556*.
- [16] Szegedy, C., Liu, W., Jia, Y., Sermanet, P., Reed, S., Anguelov, D., Erhan, D., Vanhoucke, V., and Rabinovich, A. "Going deeper with convolutions." Proc., Proceedings of the IEEE Conference on Computer Vision and Pattern Recognition, 1–9.
- [17] He, K., Zhang, X., Ren, S., and Sun, J. "Deep residual learning for image recognition." Proc., Proceedings of the IEEE Conference on Computer Vision and Pattern Recognition, 770–778.
- [18] Huang, G., Liu, Z., Van Der Maaten, L., and Weinberger, K.Q. "Densely connected convolutional networks." Proc., Proceedings of the IEEE Conference on Computer Vision and Pattern Recognition, 4700–4708.
- [19] F.N. Iandola, S. Han, M.W. Moskewicz, K. Ashraf, W.J. Dally, K. Keutzer, SqueezeNet: AlexNet-level accuracy with 50x fewer parameters and < 0.5 MB model size, *arXiv preprint arXiv:1602.07360* (2016).
- [20] Chollet, F. "Xception: deep learning with depthwise separable convolutions." Proc., Proceedings of the IEEE Conference on Computer Vision and Pattern Recognition, 1251–1258.
- [21] A.G. Howard, M. Zhu, B. Chen, D. Kalenichenko, W. Wang, T. Weyand, M. Andreetto, H. Adam, Mobilenets: efficient convolutional neural networks for mobile vision applications, *arXiv preprint arXiv:1704.04861* (2017).
- [22] Sandler, M., Howard, A., Zhu, M., Zhmoginov, A., and Chen, L.C. "Mobilenetv2: inverted residuals and linear bottlenecks." Proc., Proceedings of the IEEE Conference on Computer Vision and Pattern Recognition, 4510–4520.
- [23] Zhang, X., Zhou, X., Lin, M., and Sun, J. "Shufflenet: an extremely efficient convolutional neural network for mobile devices." Proc., Proceedings of the IEEE Conference on Computer Vision and Pattern Recognition, 6848–6856.
- [24] M.X. Tan, Q.V. Le, EfficientNet: rethinking model scaling for convolutional neural networks, *Pr Mach Learn Res* 97 (2019).
- [25] Z. Dahou, Z.M. Sbartai, A. Castel, F. Ghomari, Artificial neural network model for steel-concrete bond prediction, *Eng. Struct.* 31 (8) (2009) 1724–1733.

- [26] I.C. Yeh, Modeling of strength of high-performance concrete using artificial neural networks, *Cement Concr. Res.* 28 (12) (1998) 1797–1808.
- [27] E. Figueiredo, G. Park, C.R. Farrar, K. Worden, J. Figueiras, Machine learning algorithms for damage detection under operational and environmental variability, *Struct. Health Monit.* 10 (6) (2011) 559–572.
- [28] M. Flah, I. Nunez, W. Ben Chaabene, M.L. Nehdi, Machine learning algorithms in civil structural health monitoring: a systematic review, *Arch Comput Method E* 28 (4) (2021) 2621–2643.
- [29] Y.J. Cha, K. You, W. Choi, Vision-based detection of loosened bolts using the Hough transform and support vector machines, *Autom. ConStruct.* 71 (2016) 181–188.
- [30] Y.J. Cha, W. Choi, G. Suh, S. Mahmoudkhani, O. Buyukozturk, Autonomous structural visual inspection using region-based deep learning for detecting multiple damage types, *Comput.-Aided Civ Inf* 33 (9) (2018) 731–747.
- [31] Y.Q. Gao, K.M. Mosalam, Deep transfer learning for image-based structural damage recognition, *Comput.-Aided Civ Inf* 33 (9) (2018) 748–768.
- [32] F. Kucuksubasi, A.G. Sorgucb, Transfer Learning-Based Crack Detection by Autonomous UAVs, 2018. *ArXiv*, abs/1807.11785.
- [33] N.D. Hoang, Q.L. Nguyen, X.L. Tran, Automatic detection of concrete spalling using piecewise linear stochastic gradient descent logistic regression and image texture analysis, *Complexity* 2019 (2019).
- [34] D. Gonzalez, D. Rueda-Plata, A.B. Acevedo, J.C. Duque, R. Ramos-Pollan, A. Betancourt, S. Garcia, Automatic detection of building typology using deep learning methods on street level images, *Build. Environ.* 177 (2020).
- [35] S. Naito, H. Tomozawa, Y. Mori, T. Nagata, N. Monma, H. Nakamura, H. Fujiwara, G. Shoji, Building-damage detection method based on machine learning utilizing aerial photographs of the Kumamoto earthquake, *Earthq. Spectra* 36 (3) (2020) 1166–1187.
- [36] G. Dogan, M. Hakan Arslan, A. Ilki, Detection of damages caused by earthquake and reinforcement corrosion in RC buildings with Deep Transfer Learning, *Eng. Struct.* 279 (2023).
- [37] Z.L. Bai, T.J. Liu, D.J. Zou, M. Zhang, A. Zhou, Y. Li, Image-based reinforced concrete component mechanical damage recognition and structural safety rapid assessment using deep learning with frequency information, *Autom. ConStruct.* 150 (2023).
- [38] Y.N. Du, D.C. Feng, G. Wu, InSAR-based rapid damage assessment of urban building portfolios following the 2023 Turkey earthquake, *Int. J. Disaster Risk Reduc.* 103 (2024) 104317.
- [39] N. Bektaş, O. Kegyes-Brassai, Enhancing seismic assessment and risk management of buildings: a neural network-based rapid visual screening method development, *Eng. Struct.* 304 (2024).
- [40] AQSIQ-PRC, AQSIQ-PRC. Classification of Earthquake Damage to Buildings and Special Structures GB/T 24335, General Administration of Quality Supervision, Beijing, 2009. Inspection and Quarantine of the People's Republic of China; 2009. (in Chinese).
- [41] MHURD-PRC, "MHURD-PRC. Technical Specification for Post-earthquake Urgent Assessment and Repair of Buildings JGJ/T415, Ministry of Housing and Urban-Rural Development of the People's Republic of China, Beijing, 2017, 2017. (in Chinese).".
- [42] Y. Gao, K.M. Mosalam, PEER Hub ImageNet: a large-scale multiattribute benchmark data set of structural images, *J. Struct. Eng.* 146 (10) (2020).
- [43] G. Huang, Y. Sun, Z. Liu, D. Sedra, K.Q. Weinberger, Deep networks with stochastic depth, *Lect. Notes Comput. Sci.* 9908 (2016) 646–661.
- [44] J. Hu, L. Shen, G. Sun, Squeeze-and-Excitation networks, *Proc Cvpr Ieee* (2018) 7132–7141.
- [45] C. Liu, S.M.E. Sepasgozar, Q. Zhang, L. Ge, A novel attention-based deep learning method for post-disaster building damage classification, *Expert Syst. Appl.* 202 (2022).
- [46] MOT-PRC, MOT-PRC. Specifications for Maintenance of Highway Bridges and Culverts JTG 5120-2021, Ministry of Transport of the People's Republic of China, Beijing, 2021.
- [47] D.C. Feng, W.J. Wang, S. Mangalathu, Z. Sun, S. Mukhopadhyay, Condition assessment of highway bridges using textual data and Natural Language Processing-(NLP-) based machine learning models, *Struct. Control Health Monit.* 2023 (2023) 1–17.
- [48] Ang, A.H., Kim, W.J., and Kim, S.B. "Damage estimation of existing bridge structures." Proc., Structural Engineering in Natural Hazards Mitigation, ASCE, 1137–1142.
- [49] A. Colombo, P. Negro, A damage index of generalised applicability, *Eng. Struct.* 27 (8) (2005) 1164–1174.
- [50] EERI, Expected Seismic Performance of Buildings, Earthquake Engineering Research Institute, 1994.
- [51] A. Ghobarah, H. Abou-Elfath, A. Biddah, Response-based damage assessment of structures, *Earthq. Eng. Struct. Dynam.* 28 (1) (1999) 79–104.
- [52] W.C. Stone, A.W. Taylor, Seismic Performance of Circular Bridge Columns Designed in Accordance with AASHTO/CALTRANS Standards, 1993.